Research Article

Wanli Ma, Fenghe Tao*, Changzhi Jia, and Xiangdong Men

Research on microstructure and forming mechanism of TiC/1Cr12Ni3Mo2V composite based on laser solid forming

https://doi.org/10.1515/phys-2019-0036
Received Apr 10, 2019; accepted Apr 30, 2019

Abstract: Samples of 1Cr12Ni3Mo2V-based composites with different TiC contents (The volume fraction of TiC were 0%, 10%, 20%, 30%, 40%) were prepared based on laser solid forming. Thermodynamic analysis was performed to estimate the possible chemical reactions. Phase analysis and microscopic topography analysis were characterized by optical microscopy (OM), scan electron microscopy (SEM), X-ray diffraction (XRD) and energy dispersive X-ray analysis (EDS). Finally, the formation mechanism of microscopic appearance was analyzed. The results indicate that the TiC particles were successfully dispersed in the matrix. TiC particles mainly exist in two ways in the matrix. The large particles were not completely melted and the small particles were decomposed and then precipitated. Their shape was mainly cross, plum-shaped or dendritic distribution with different TiC contents.

Keywords: laser solid forming; 1Cr12Ni3Mo2V steel; wear resistance; microstructure

PACS: 28.52.Fa, 81.05.Bx, 81.20.Ev

1 Introduction

Laser solid forming technology is an additive manufacturing technology. Unlike traditional manufacturing techniques, this technology is processed in layers. Laser solid forming technology has the following advantages such as fast processing speed and saving raw materials [1–3]. What is more, complex structural parts can be processed. At present, the technology is already widely used in the aerospace, automotive, and abrasive industries.

The unique advantages of laser solid forming have broad application prospects in equipment support. At present, titanium alloy and nickel-based alloy are the main manufacturing materials for laser solid forming [4, 5]. But these materials are not suitable for weaponry because of performance and economic issues. Some materials that are similar in performance to weapon system materials and inexpensive are required to be studied.

Particle reinforced metal matrix composites have high strength, high melting point and good wear resistance. Furthermore, the preparation process of the material is simple and low in cost. 1Cr12Ni3Mo2V is selected as the matrix, because the performance is similar to that of the weapon parts. When selecting a particle, it is necessary to consider its preparation process and production cost and other factors. Currently, the main enhancement phase particles include TiC, SiC, WC, Al_2O_3 and SiO_2 [6, 7]. Table 1 shows the material properties. The better the wettability of particles and iron, the better the combination [8, 9]. WC particles are completely wetted with iron and have a zero wetting angle. But the newly formed WC particles are easily dissolved in the iron matrix gap which leads to difficult control of the preparation process [10]. The wetting angle between TiC and iron is small and the reaction is stable. Simultaneously the thermal expansion coefficient of titanium is close to iron. TiC is used as a reinforcing phase particle.

Table 1: Material properties of enhanced phase

Materials	Density (g/cm^3)	Melting point (K)	Thermal expansion coefficient ($10^{-6}{}^{\circ}C^{-1}$)	Elastic Modulus (GPa)
TiC	4.99	3244	6.5	440
SiC	3.19	2970	4.6	430
WC	15.60	2870	5.2	713
Al_2O_3	3.90	2050	9.0	360

***Corresponding Author: Fenghe Tao:** Army Engineering University, Shijiazhuang, China; Email:qfyykym@163.com
Wanli Ma: Army Engineering University, Shijiazhuang, China; Email: lwyx2018@163.com
Changzhi Jia: Army Engineering University, Shijiazhuang, China; Email: chaoyang@126.com
Xiangdong Men: Army Engineering University, Shijiazhuang, China; Email: xdmen2016@163.com

Table 2: Stainless steel composition

C	Mn	Si	S	P	Cr	Ni	Mo	V
0.11	0.56	0.64	0.01	0.015	11.5	2.5	2.12	0.27

In this paper, firstly a thermodynamic analysis was performed to estimate the possible chemical reactions. The order of possible chemical reactions was determined based on the principle of free energy determination. Then different content of TiC composites were prepared (volume fraction of TiC are 0%, 10%, 20%, 30%, 40%). Phase analysis was carried out for different samples to determine the specific product. Then microscopic analysis was conducted and the morphology of different samples comparatively analysed. Finally, the formation mechanism of microscopic topography is analyzed.

2 Experimental materials and methods

The matrix material selected in the experiment is 1Cr12Ni3Mo2V steel for its good mechanical properties. The main components of 1Cr12Ni3Mo2V stainless steel are shown in Table 2. The particle size of steel powder is 10-50um. Enhanced phase particles are TiC and the particle size is 10-50um.

Experimental parts are processed on laser solid forming equipment. The laser solid forming system mainly includes laser system, powder feeding system, numerical control system and gas protection system, etc. The powder feeding system has two cylinders respectively placing TiC powder and 1cr12ni3mo2v powder. Change the material ratio by changing the rate of powder feeding of the two powders. The test specimens with TiC volume fraction of 0%, 10%, 20%, 30% and 40% were made, respectively. The powder is dried by 120°C heat Preservation 1 h in the vacuum drying chamber before the specimen is processed. Other parameters of the laser solid forming system are as follows: Laser power set to 800W, scanning rate is 600 mm/min, powder feeder protection gas is 6 l/min. The size of the manufactured part is $8 \times 8 \times 8$ [cm^3]. Then the manufactured parts were characterized by optical microscopy (OM), scan electron microscopy (SEM), X-ray diffraction (XRD) and energy dispersive X-ray analysis (EDS).

3 Results

3.1 Thermodynamic analysis

The occurrence of chemical reactions is mainly determined by the thermodynamic properties of the participating reactants. Generally, the possibility of reaction can be judged theoretically according to the free energy, entropy and enthalpy in the thermodynamic function. At present, the main principle is to use free energy as a criterion. The thermodynamic function is expressed as follows:

$$\Delta G = \Delta H - T \cdot \Delta S \tag{1}$$

ΔG is Gibbs free energy, the unit is $J \cdot MOL^{-1}$. ΔH is enthalpy, the unit is $J \cdot MOL^{-1}$. ΔS is entropy value, the unit is $J \cdot Mol^{-1} \cdot k^{-1}$. T is temperature, K is unit.

Depending on the numerical of the ΔG, it can be judged whether a chemical reaction can be carried out. When $\Delta G>0$, the chemical reaction cannot be carried out spontaneously. When $\Delta G<0$, the chemical reaction can proceed spontaneously. Based on the main components of the matrix and ceramic particles, it is speculated that the following reactions occur mainly by consulting the relevant thermodynamics manual. The magnitude of the reaction trend ability can also be judged by calculating the magnitude of ΔG. The smaller the $|\Delta G|$, the smaller the reaction tendency ability.

The transient temperature of the laser spot can reach 3000°C. The reaction can occur TiC=Ti+C. The C element itself is relatively active and can react with various elements. Possible reactions are as follows:

$$Ti + C = TiC \tag{2}$$

ΔG=-186606+13.2T

$$3Fe + C = Fe_3C \tag{3}$$

ΔG=25920-23T 298K<T<493K
ΔG=26670-25T 493K <T<1115K
ΔG=10340-10T T>1115K

$$2Fe + C = Fe_2C \tag{4}$$

ΔG=19860-10T 298K<T<1115K
ΔG=18420-10T T>1115K

$$2Fe + Ti = Fe_2Ti \tag{5}$$

ΔG=-53300+54T 298K<T<2000K

According to the above function, the reaction for generating TiC can be performed continuously. The condition for generating Fe_3C is T>1034K. The condition for generating Fe_2C is T>1842K. Unstable at low temperatures, the condition for the formation of Fe_2Ti is temperature T <992K. Fe_2Ti is an unstable phase at high temperatures. Since the temperature of the molten pool at the time of laser spot irradiation is much higher than the temperature at which the reaction occurs, it is less likely that Fe_2Ti will be present.

According to the principle of determination of free energy: The order of the reaction is TiC>Fe_2Ti>Fe_3C. Fe_2Ti is unstable in the molten pool and there may be less. As the temperature increases, Ti and C react preferentially to form TiC with stable properties. The reaction rate increases with increasing temperature, allowing Ti+C=TiC to react adequately. If there is no residual Ti and C in the system after the reaction, only TiC and Fe are present in the reacted matter. When Ti remains after the reaction, excess Ti reacts with Fe to preferentially form Fe_2Ti. An increase in temperature also exacerbates the formation of Fe_2Ti. When the reaction 2Fe+C=Fe_2C occurs completely, the temperature is continuously increasing and Ti and Fe will continue to react. Fe acts only as a medium when reacting with Ti and C. When the reaction C has surplus, the excess C will react with Fe, and when the temperature is above 1034K, C will react with Fe. If Ti and C fully react before 1034K, at this point C and Fe are only conducting diffusion motions because C and Fe do not meet the required reaction temperature. If Ti and C are completely reactive after 1034K, then the extra C will react immediately to Fe and generate Fe_3C.

3.2 Material Phase Analysis

Figure 1 shows the XRD results of matrix and composite. Compared with the matrix composition, it is obvious that TiC exists in the composite achieving the purpose of combining TiC with the matrix. Ti element mainly exists in the form of TiC. The two substances, Fe_3C and Fe_2C, are not generated in the matrix and the generation of harmful phases is reduced. Chemical reactions (3) and (4) did not occur. It has positive effect on performance optimization of composite materials.

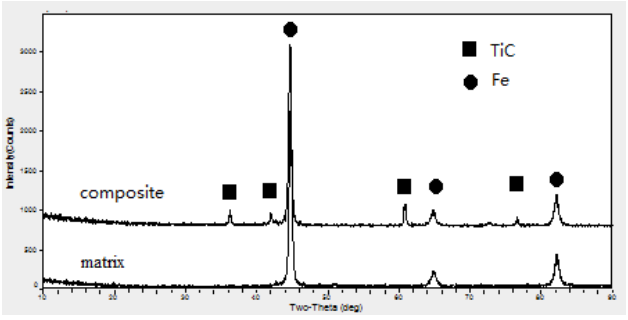

Figure 1: XRD results of matrix and composite

3.3 Microscopic topography analysis

The TiC content of the test pieces no. 1 to no. 5 is 0, 10%, 20%, 30% and 40%. The test piece no. 1 is a comparative piece which is the matrix. There is no ceramic particles added in the part. It can be seen in the Figure 2, that the matrix structure is uniform and there are no other impurities.

The Figure 3 shows the microscopic picture of piece no. 2 with the 10% TiC. It can be seen that large gray particles appear on the substrate. These particles are irregular in shape and have a certain degree of segregation in the distribution. The particle size is close to the TiC particle size in the raw material. The matrix color is deeper than piece no 1. Partially magnifying the substrate it can be seen that there are more gray small particles in the matrix. They are mainly round or cross and more evenly distributed.

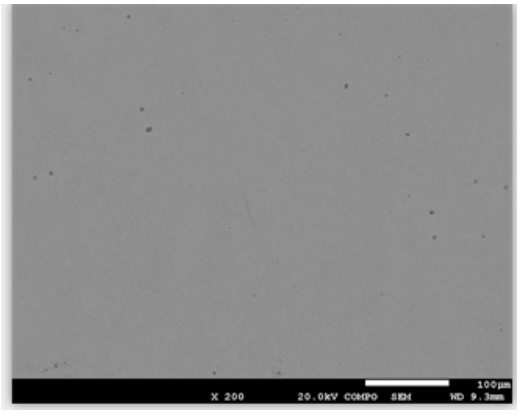

Figure 2: Matrix microstructure

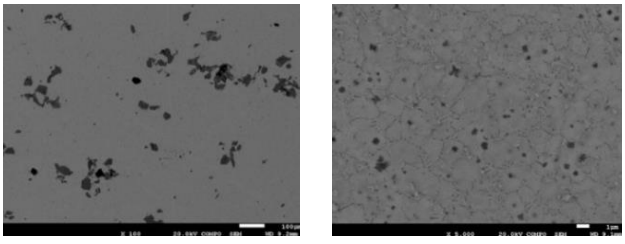

Figure 3: 10% TiC micromorphology and partial enlargement

Partial magnification of large particles is shown in the Figure 4. The large particle shape is irregular and they are divided by multiple white lines. It characterizes the melting mode of large particles. EDS experimental analysis of large particles is carried out. It is obvious that the atomic ratio of Ti and C is close to 1:1. It can be seen that the main component of large particles is TiC. At the same time, according to the size of the large particles, it can be judged that these large particles are incompletely melted TiC particles.

Small particles were analyzed by EDS as in the Figure 5. The presence of Ti in small particles was observed. And Fe, Cr, Mn, Ni and other elements belong to the matrix. Since the small particle size is too small, part of the matrix is included in the EDS analysis. Since the matrix is martensitic stainless steel and the amount of C in the matrix is high, the content of C in the EDS test is greater than the content of Ti. In combination with the previous XRD analysis, there is no carbide formation of Fe and Cr, and it can be judged that the small particles are TiC particles.

The Figure 6 below shows the microscopic topography of the no. 3 piece with 20% TiC content, which produces large gray particles with irregular shapes. The particle distribution is relatively uniform. The size is similar to that of the no. 2 piece, and the quantity is higher. The color of the base is deeper than that of the no. 2 piece. The matrix is partially enlarged as in the Figure 6 and there are small gray particles in the matrix. The shape is mainly plum-shaped and cross-shaped. A small number of circles has a relatively even distribution and a larger size than that of no. 2 piece. EDS analysis of large and small particles also shown that the particles are TiC.

The Figure 7 shows the microscopic topography of the no. 4 piece, which produces large gray particles with irregular shapes. Large particle distribution is uneven. The size is similar to that of the no. 2 piece, and the quantity is less than the no. 3 piece. The color of the matrix is deeper than that of the no. 3 piece. The matrix is partially enlarged and there are small gray particles in the matrix. The shape is mainly dendritic. The size of small particles is larger than the no. 3 piece. EDS analysis of large and small particles also obtained size particles are TiC particles.

The Figure 8 shows the microscopic topography of the no. 5 piece with 40% TiC, which produces large gray particles with irregular shapes. The size is similar to that of the no.2 piece and the quantity is similar to the no. 2 piece. The color of the matrix is deeper than that of the no. 4 piece. The matrix is partially enlarged and there are small gray particles in the matrix. The shape is mainly dendritic and

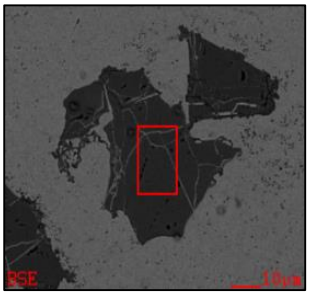

Element	Wt%	At%
CK	15.09	41.69
TiK	79.79	55.25
CrK	00.51	00.33
FeK	04.60	02.73
Matrix	Correction	ZAF

Figure 4: Large particle composition

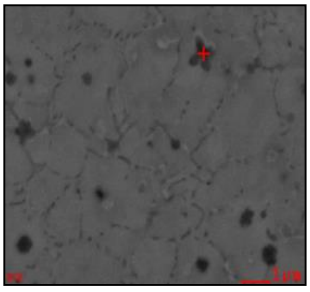

Element	Wt%	At%
CK	08.00	28.49
MoL	02.18	00.97
TiK	10.07	08.99
CrK	09.09	07.48
MnK	00.74	00.58
FeK	67.27	51.54
NiK	02.67	01.94
Matrix	Correction	ZAF

Figure 5: Small particle component

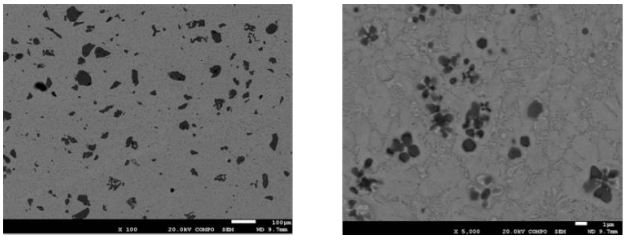

Figure 6: 20% TiC micromorphology and partial enlargement

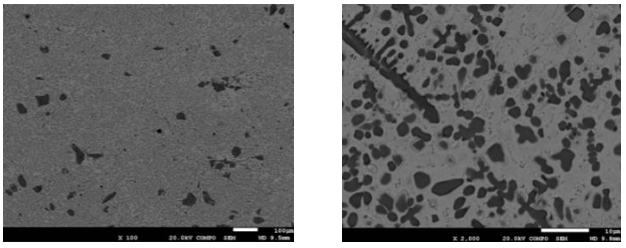

Figure 7: 30% TiC micromorphology and partial enlargement

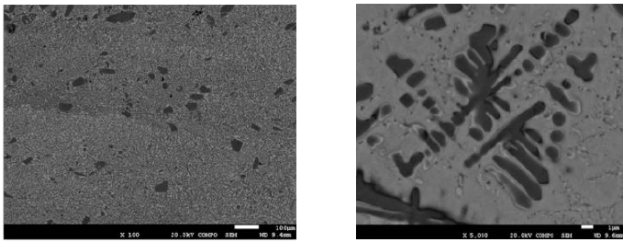

Figure 8: 40% TiC micromorphology and partial enlargement

plum blossom. The distribution is relatively uniform and the dendrite size is larger than that of the no.4 piece. Similarly, both large and small particles are TiC particles.

3.4 Formation mechanism analysis

It can be seen from Figure 3, 6, 7 and 8 that as the volume fraction of TiC increases, the re-precipitated TiC produces a process from circular to cruciform to plum-shaped to dendritic. The causes of phase transitions are analysed as follows. The initial TiC particles are decomposed in the molten pool to form Ti atoms and C atoms, when the laser is irradiated to the TiC particles. During the formation of the molten pool and the maintenance of the liquid phase, the above metallurgical reaction begins and proceeds according to its own thermodynamic conditions. At this point, the reaction begins to form a stable crystal nucleus. As the reaction time prolongs, the crystal nucleus continues to form, which causes the content of Ti and C in the molten pool to drop continuously. When the atomic concentration falls below the critical concentration required for the application, the substance produced by the new reaction cannot exist in the form of a stable crystal nucleus. It can only accumulate and grow up on the generated crystal nucleus according to the preferential growth direction of the crystal and the cross shape, plum shape, and dendritic shape gradually formed.

The growth of TiC crystals is affected by many aspects. At the beginning of the chemical reaction, TiC continuously synthesizes and forms crystal nuclei. Because the reaction Ti+C=TiC is an exothermic reaction and a large amount of latent heat of crystallization is released while crystallizing. At the same time, various forces in the molten pool affect the crystals. The heat conduction process in the molten pool along the printing direction has a certain directionality causing the continuously formed crystal nucleus to nucleate in the dendritic direction in the molten pool. Due to the continuous formation of crystal nuclei, the atomic concentration around the nucleus is continuously decreasing. And the concentration along the direction in which the crystal nuclei are arranged is the lowest, and the growth rate is also the slowest. On the side of the alignment direction, due to the small number of crystal nuclei, the surrounding Ti and C atoms will first diffuse here. A difference in concentration around the nucleus is formed resulting in subcooling, which causes the particles to grow slowly along the branches and grow faster in the lateral direction. This forms the side growth mode. Figure 9 shows the dendritic formation. The first stage is continuous nucleation and crystal nucleus arrangement is as in Figure 9(a). The second stage is that the crystal nucleus continues to grow and generate new crystal nucleus just as the shape in Figure 9(b). The third stage is that the nascent TiC grows up on the side as the shape in Figure 9(c).

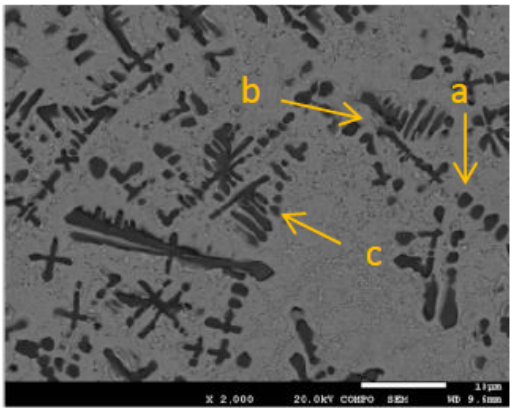

Figure 9: Different crystal morphology

4 Conclusions

(i) The metal matrix composite was prepared by laser solid forming and the TiC particles were successfully dispersed in the matrix. TiC particles mainly exist in two ways in the matrix. Large particles are TiC that are not completely melted and small particles are TiC that are decomposed and regenerated.

(ii) The microstructures with different TiC contents are compared and forming a cross, plum-shaped, gradually dendritic distribution. As the TiC content increases, the number of incompletely decomposed TiC particles first increases and then decreases. The composite with 20% TiC has the highest number of large TiC. As the TiC content increases, the amount of regenerated small TiC increases.

(iii) The formation of dendrites is mainly divided into three stages. The first stage is continuous nucleation. The second stage is that the crystal nucleus continues to grow and generate new crystal nucleus. The third stage is that the nascent TiC grows up on the side.

References

[1] Yuan T., Cai Y.C., Luo Z., Chao Y.J., Zeng Y.D., Effect of Al_2O_3 Composite Ceramic Reinforcement on Wear Behavior of Laser Cladding Ni-Based Alloys, J. Shanghai Jiaotong Univ., 2016, 50(10), 1635-1639.

[2] Zhao Y.B., Chen W.Q., An Q.L., Surface Morphology Simulation and Experimental Study of Grinding for Ceramic Particles Reinforced Ti, Aerospace Manufacturing Technology, 2017, 05, 8-14.

[3] Cheng S.L., Zhong L.S., Fu Y.H., Development of Tungsten Carbide Particulate Reinforced Steel Matrix Composite, Hot Working Technology. 2014, 43(18). 9-12.

[4] Liu Q.M., Current Status of Laser Cladding Ceramic Reinforced Metal Matrix Composite Coating, Thermal Spray Technology. 2014, 6(2), 1-5.

[5] Jin Y.H., Bi S., Wu Y.W., Lu X.T., Effect of TiC mass-fraction on microstructure and performance of WC-Co composite coating prepared with laser melt-cladding, Journal of Lanzhou University of Technology. 2018, 44(6), 12-16.

[6] Tang Y.Y., Yuan S.Q., Yang P., Yang L., Feng L., Effects of cladding surface treatment technology on the performance of Titanium alloy, Special-cast and Non-ferrous Alloys. 2018, 38(11), 1204-1207.

[7] Xu B., Lian B.X., Han J.X., Study on laser cladding coating and mechanical properties of high speed steel cutting tools, Foundry Technology, 2018, 39(03), 707-710.

[8] Li L.U., Wang Q.M., Chen B.Z., Microstructure and cutting performance of Cr-Ti-A-N coating for high-speed dry milling, Transactions of Nonferrous Metals Society of China. 2014, 24(6), 1800-1806.

[9] Chi J., Li M., Wang S.F., Wu J., Effects of TiC Formation Modes on Microstructure and Performance of Ni-based Laser Cladding Coatings, China Surface Engineering. 2017, 30(04), 134-171.

[10] Tang J.M., Mechanical and tribological properties of the Ti C-Ti B2 composite coating deposited on 40Cr-steel by electro spark deposition, Applied Surface Science. 2016, 365, 202-208.